GNSS RO refractivities as a climate change measure

Henrik Vedel (hev@dmi.dk) and Martin Stendel (mas@dmi.dk)
Danish Meteorological Institute, Lyngbyvej 100, DK 2100 Copenhagen, Denmark

Abstract. Global Navigation Satellite System (GNSS) Radio Occultation (RO) measurements potentially provide bias free, time stable atmospheric observations, useful in both climate monitoring and numerical weather prediction (NWP).

In simplified terms the GNSS RO observations can be used to determine profiles of temperature and humidity, somewhat like a radio-sounding. However, the original GNSS RO observables do not correspond to traditional meteorological variables. Various degrees of preprocessing are necessary before the data can be utilised in meteorology. Inevitably this involves assumptions and/or use of other data, e.g. from climatology or NWP, which may lead to a degradation of the quality.

While some of the preprocessing can be avoided by including the GNSS RO data in (re)analyses it will take awhile, before such re-analysis data become available.

In this article we consider a more direct use of GNSS RO data, by investigating how sensitive GNSS RO data in a more "raw" format, i.e. *not* processed into temperature and humidity, are to climate change. We find that the GNSS RO product refractivity as function of height is as sensitive to climate change as are traditional measures like the geopotential height or temperature of pressure surfaces. In the stratosphere the heights of iso refractivity surfaces appear even more sensitive to climate change than the heights of isobaric surfaces. The GNSS RO observations are totally independent of other atmospheric observations, which makes them not only highly useful for climate monitoring purposes and climate change detection, but also makes them an ideal tool for the verification of results based on other observational datasets and/or re-analysis data.

Additionally, it is found that GNSS observations obtained from ground, in the form of zenith total delays, are well suited for climate research.

Keywords: GNSS; refractivity; geopotential height; ZTD; climate monitoring

Submitted to Climatic Change

1. Introduction

In the atmosphere of Earth the speed of radio-waves is reduced relative to its vacuum value. In combination with the inhomogeneity of the atmosphere this causes the radio-waves emitted from GNSS satellites to bend when passing the atmosphere. The corresponding time delay and bending, relative to a no atmosphere situation, is measurable. The effect depends on the density and the electromagnetic properties of the species interacting with the radio-waves. It is strongest in the ionosphere, but noticeable also further down in the neutral atmosphere,

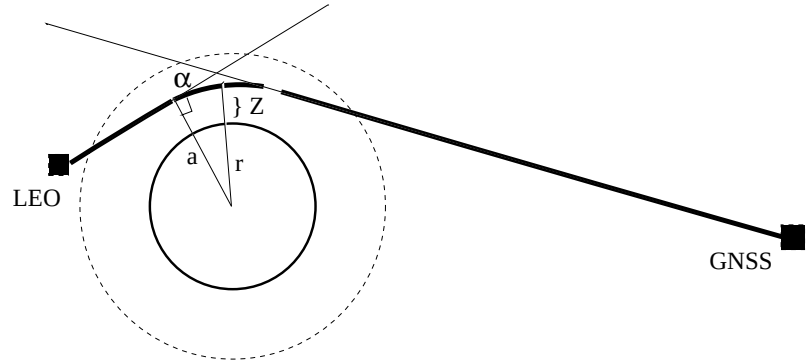

Figure 1. The occultation measurement geometry

where water vapour molecules interact particularly strong relative to the dry air molecules, due to their dipole moment.

GNSS RO observations are made by having a GNSS receiver on board a low earth orbit (LEO) satellite record the arrival time and frequency of radio-signals emitted by an occulting GNSS satellite. Combined with precise knowledge of the time of emission and the orbits of the satellites involved this enables determination of the net effect of the atmosphere upon the radio-signals.

From the observations it is possible to derive the *bending angle*, α, representing the difference in direction of the radio-signals emitted and received. Based on an assumption about local spherical symmetry, on can further determine the impact parameter (see Fig. 1 for definitions). Use of dual frequency GNSS receivers enables removal of the dominant ionospheric component, which is dispersive, leaving us with the change in angle due to the lower, neutral atmosphere. It is this, remainder, bending angle we shall be referring to in all of the following. This bending angle versus impact parameter is one type of GNSS RO product which will become available to meteorologists in the future.

Assuming local spherical symmetry the bending angle as function of impact parameter, a, is given by (Meincke, 1999):

$$\alpha = -2a \int_r^\infty (r^2 n^2 - a^2)^{-1/2} \frac{d \ln n(r)}{dr} dr, \tag{1}$$

where n is the refractive index. n is very close to one, and it is customary to introduce instead the refractivity $N = (n-1)10^6$. Thus, using an Abel transformation, the bending angle profile can be converted to a profile of refractivity versus impact parameter, which is related to geometric height, Z, via,

$$a = (1 + 10^{-6} N)(R_e + Z) \tag{2}$$

where R_e is the local radius of curvature. Refractivity as function of height is another product which will become available from GNSS RO observations.

The term 'height' is used differently in geodesy and meteorology. To avoid confusion and errors when this is not properly appreciated we here give a detailed description, well knowing that this is basic knowledge to some.

The heights mentioned above are determined relative to an ellipsoid representing the surface of the Earth. They may be converted to heights relative to the geoid, which corresponds to the zero height reference surface normally used in meteorology (common topographic maps, etc.). The geometric height is related to the geopotential height, h, via $g\delta z = g_0 \delta h$, where g is the acceleration due to gravity and non inertial forces on a particle at rest and g_0 is a constant. Geopotential height is the most common height measure in meteorology.

Assume the atmosphere is hydrostatic, which is a very fine approximation on the scales of interest here. Then $\delta p = -g\rho\delta z$, where ρ is the matter density and p is the pressure. Using the equation of state of an ideal gas, $p = \rho RT$, T being temperature and R the gas-constant, and considering the atmosphere to consist of a mixture of two ideal gases: dry air and water vapour, where the amount of the latter is described by the specific humidity, $q \equiv \rho_w/\rho$, with $\rho \equiv \rho_w + \rho_d$ and subscripts w and d stands for water vapour and dry air respectively, we get:

$$\frac{1}{g_0} R_d T(1 + q(1/\epsilon - 1)\delta \ln p = -\delta h = -\frac{g}{g_0}\delta z, \tag{3}$$

where R_d is the gas constant for dry air and ϵ is the ratio of the molecular mass of water vapour to that of dry air. The benefit of using geopotential heights in meteorology is that one need not operate with a gravitational field varying in space when estimating heights. The price is that geopotential heights are not proper heights, and less used in most other fields of physics. It is straight-forward, however, to transform between the different types of heights and reference surfaces (at the precision needed for meteorological purposes). Though one should notice that the definition of geopotential height used in most numerical weather prediction models, and inherited from there to climate models as well, differs slightly from the textbook definition and is model dependent (e.g. Vedel, 2000).

For the present study we use geopotential height as our height variable, as it is most easily obtained from the climate model data and it does not limit the usefulness of our findings. The relation between geometric and geopotential height does not change in response to global warming. It is related only to the field of gravity of the Earth, and the

very minor changes in atmospheric structure due to for example global warming can be safely ignored in that regard.

Refractivity is related to the density of the interacting molecules through an empirical relation,

$$N = R_d \rho_d k_1 + R_w \rho_w k_2 + R_w \rho_w k_3 / T. \tag{4}$$

The k's are a set of empirically determined constants. See e.g. Bevis et al. (1994) for a discussion of their values. For this study we use: $k_1 = 7.76\ 10^{-7}$K/Pa, $k_2 = 7.04\ 10^{-7}$K/Pa, and $k_3 = 3.739\ 10^{-3}$K^2/Pa.

Using the equation of state we can rewrite this,

$$N = \rho R_d (k_1 + \frac{q}{\epsilon}[k_2 - k_1/\epsilon] + \frac{k_3}{T}) \tag{5}$$

$$= \frac{p}{T} \frac{1}{1 + q(1/\epsilon - 1)} (k_1 + \frac{q}{\epsilon}(k_2 - k_1/\epsilon + \frac{k_3}{T})). \tag{6}$$

Eq. 6 shows why refractivities are potentially useful for climate monitoring, being related to key meteorological variables: pressure, temperature, and humidity.

Consider a level high in the atmosphere, e.g. at 40 km. Here the air is totally dry, consequently Eq. 3 and 6 in combination can be used to determine a profile of pressure and temperature based on an observed refractivity profile. The downward integration of the hydrostatic equation requires an assumption about the upper boundary condition, i.e. the pressure or temperature at a certain height. One can show, however, that provided this assumption is made high above the region of interest the relative error becomes negligible further down (Leroy, 1997). This is due to the strong, approximately exponential, increase in density down through the atmosphere, which, in relative terms, dominates the error.

When humidity is not negligible, in terms of its contribution to the local refractivity, auxiliary information is needed in order to solve the so-called temperature/humidity degeneracy. Different methods are being invented and tested for this purpose (see e.g. Kuo (2000) and Healy and Eyre (2000) and references in those). Some rely on climatological constraints, some on current temperature information from a NWP model or other sources. The currently best methods do the conversion implicitly, by means of 1D variational data assimilation of refractivity into a model in which the first guess temperature and humidity profile is provided by e.g. an NWP model. The benefit of using variational data assimilation is that it balances in a proper way the statistical errors of the observations and of the first guess data providing the auxiliary information. This points toward 3 and 4D variational data assimilation of refractivity being the optimal way in which to use GNSS

RO observations for NWP and climate work in the future. Development of such routines is under way, enabling future direct inclusion of GNSS RO refractivity data in NWP data assimilation and re-analyses. (From certain viewpoints bending angle might be even better, but direct assimilation of bending angle is currently too expensive cpu wise for operational use, see e.g. Zou et al. (2000).

From Eq. 5 we see that the fractional error from neglecting humidity in the density deduced is,

$$\frac{\rho(q=0)-\rho}{\rho} = (\frac{k_2}{k_1} - 1 + \frac{k_3}{k_1 T})\frac{q}{\epsilon} \quad (7)$$

$$\approx 28.2\ q, \qquad \text{for } T = 273K. \quad (8)$$

Because water vapour interacts much more strongly, density wise, with the GNSS radio-waves than the dry atmosphere, even a rather modest amount of specific water vapour can turn into a important miscalculation of atmospheric density if ignored. Thus, the "common knowledge" among meteorologist about when and where to ignore water vapour may not always hold when processing refractivity measurements.

It is very difficult to estimate the heights at which water vapour becomes important when using GNSS RO data. One should recall here that few high precision observations of water vapour are available above the tropopause. Correspondingly the model humidities at these levels may not be precise. Caution is therefore required when processing GNSS RO data in the lower stratosphere based on assumptions about the amount of humidity. (In the future assimilation of GNSS RO data into NWP models may help enlighten that problem.)

The integral of refractivity along the path travelled by the radio-waves, $N\delta l$, where δl is locally parallel to the ray-path, corresponds to the total delay of the signals, relative to what is expected in a vacuum situation. Notice that even though it is named a 'delay' it is measured as a distance, representing the apparent excess path corresponding to the actual time delay. Part of this excess path is real, as the rays are bend, part of it is apparent, as the rays are slowed down by the atmosphere.

Ground based GPS receivers are sensitive to these delays. Indeed, in high precission positioning, part of the data processing is to estimate and correct for them, as they represent a noise term in the problem. Currently this is done in a statistical manner, in order to stabilize the solution and overcome various other noise terms in the problem. After all a GPS receiver sees only a limited number of GPS satellites at any given time, this will improve when the European Galileo satellites are launched. In current practice one determines a single so-called zenith total delay (ZTD), which by means of mapping functions is related to the individual delays toward each of the satellites. The mapping

functions are typically based on assumptions about the atmosphere being horizontally stratified, wherefore the ZTD can be viewed as a certain type of 'average' over the actual delays, 'corrected' for the different zenith angles. Observations of ZTD are becoming available, experiments with use of the data in NWP are under way in many countries.

Based on extra information or assumptions the ZTD can be broken down into the hydrostatic delay (ZHD), which depends nearly solely on the local pressure at the GPS site, and the zenith wet delay (ZWD), which depends mainly on the column density of water vapour, but also on the temperature in that column. The ZTD may be written as,

$$ZTD = \int_{z_s}^{z_N} N \delta z \tag{9}$$

$$\approx k_1 R_d \int_0^{p_s} \frac{\delta p}{g} + \frac{R_d}{\epsilon} \int_0^{p_s} q((k_2 - k_1\epsilon) + k_3/T)\frac{\delta p}{g} \tag{10}$$

$$\equiv ZHD + ZWD \quad \text{(hydrostatic and wet delay)} \tag{11}$$

$$\approx a\ p_s/f(\theta_s, z_s) + \frac{R_d}{\epsilon g_s(\theta_s)} \sum_{i=1}^{N} q_i((k_2 - \epsilon k_1) + k_3/T_i)\Delta p_i, \tag{12}$$

where subscript s indicates site value, $a = 2.22768\ 10^{-5}$ m/Pa, and $f = 1 - 2.66\ 10^{-3} \cos 2\theta_s\ - 2.8\ 10^{-4}\text{km}^{-1} z_s$, z_s being the altitude of the site and θ_s the latitude.

In this article we use the output of a climate simulation to study the behaviour of refractivity. Therefore we are not faced with a decoupling problem for temperature and humidity.

The use of climate simulation data to estimate the usefulness of GNSS observations in climate monitoring was pioneered by Yuan et al. (1993). In the meantime the quality and resolution of climate models has improved significantly, enabling us to do a much more detailed analysis, including a study of the variations expected locally.

2. Model data and analysis

We study the expected evolution of refractivity due to climate change by means of data from a climate simulation. A number of traditional climate change measures are determined for the purpose of comparison.

The climate data come from a simulation performed with a coupled atmosphere-ocean general circulation model (AOGCM).

The atmospheric model is ECHAM4 (Roeckner et al., 1996). 19 hybrid sigma-pressure levels are used in the vertical, with the uppermost level at 10 hPa. Prognostic variables are vorticity, divergence, logarithm

of surface pressure, temperature, specific humidity, and mixing ratio of total cloud water. Variables are represented by spherical harmonics with triangular truncation at wave number 42 (T42), equivalent to a horizontal resolution of approximately 300 km.

The ocean model is an extended version of the OPYC model (Oberhuber, 1993), consisting of three sub-models: One for the interior ocean, one for the surface mixed layer, and one for the sea-ice. The ocean model has 11 layers, the horizontal resolution corresponds approximately to that of the atmospheric model. The two components are quasi-synchronously coupled and exchange information once a day. Further details about the model and the particular simulation on which the present analysis is based can be found in Stendel et al. (2000) and references therein.

The model data analysed here come for a simulation using the SRES marker scenario A2 (Nakicenovic et al., 2000). In short, such scenarios describe politically realistic future concentrations of important greenhouse gases influenced directly by humans. The scenarios have been described extensively elsewhere.

The simulation covers 110 year of climate evolution. The data extracted come from the first 10 years, which we take to represent "current" climate, and the last 10 years, which we take to represent "future" climate.

For each variable to be analysed we calculate the annual and seasonal means at 7 pressure levels between 850 and 30 hPa, at the geopotential heights between 2.5 and 22.5 km at 2.5 km steps, and at the refractivity levels: 200, 150, 100, 80, 60, 40, 30, 20, and 15 $[10^{-6}]$. Then the 10 year means and standard deviations are calculated separately for the first ten and the last ten years, and differences are deduced, as future minus current, in order to see the effects of climate change upon the variables.

The calculation of refractivity was based on Eq. 6. Increments of geopotential height were calculated using Eq. 3, which in combination with the model orography gave the total geopotential height. When interpolations were made between model levels the following relations were assumed to hold: $\delta \log p \propto \delta h$, $\delta T \propto \delta h$, and $\delta q \propto \delta h$.

ZTD and ZWD were calculated based on Eq. 12. For comparison also the more familiar quantity integrated water vapour (IWV) was calculated, as $\int \rho q \delta z \approx 1/g_s(\theta) \sum q_i \Delta p_i$.

3. Results

We here show some of the results found in the analysis of the climate simulation. While just a small subset is presented it is enough to show the main findings. The remainder data underline these.

Figures 2 and 3 show vertical cross sections of temperature and geopotential height on pressure levels. These traditional meteorological measures can be compared to the behaviour of the global means of refractivity on geopotential height surfaces (Fig. 4) and of the geopotential height on refractivity surfaces (Fig. 5).

Due to the so-called lapse-rate feedback (Tett et al., 1996; Santer et al., 1996), one expects an enhanced warming with height throughout the troposphere and a temperature decrease in the stratosphere under climate change conditions (see Fig. 2). This figure also shows the differential seasonal warming.

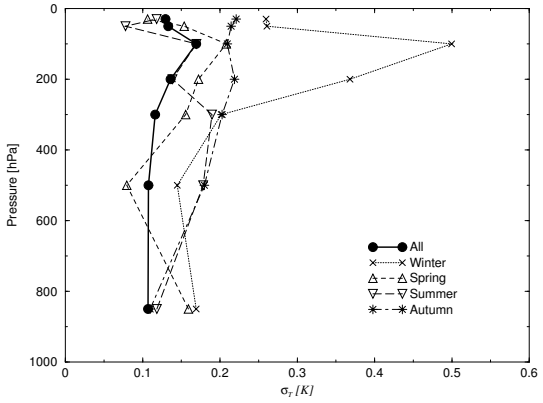

a. Inter-annual variation.

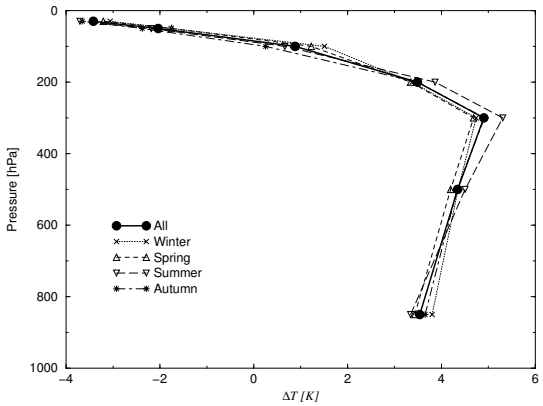

b. Climate evolution.

Figure 2. Variation of global mean temperature of pressure surfaces

Fig. 3-b shows the evolution of geopotential height according to the scenario. The increase reaches a maximum near 100 hPa. Relative to the internal inter-annual variation (Fig. 3-a), the increase is largest at the 300, 200 and 100 hPa levels.

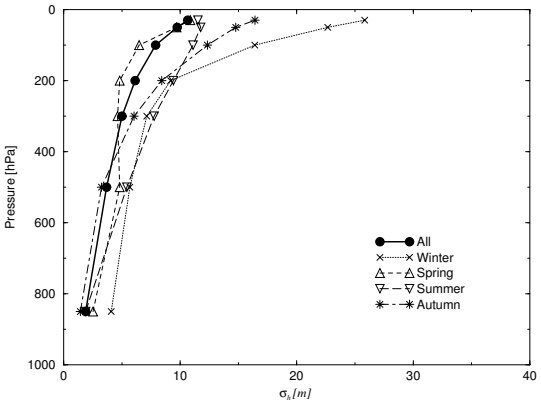

a. Inter-annual variation

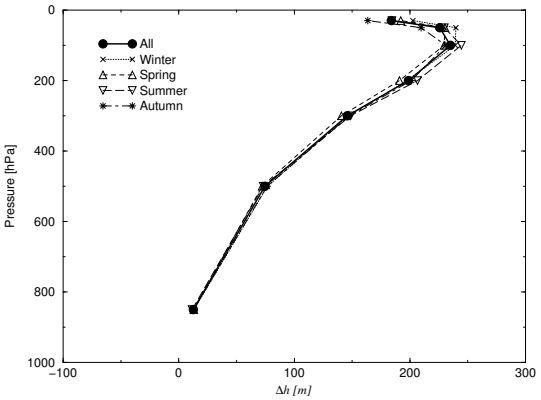

b. Future minus current.

Figure 3. Variation of global mean geopotential of pressure surfaces

Fig. 4 shows the behaviour of refractivity versus height. The global mean itself is included, Fig. 4-a, to give the reader a feeling for the vertical behaviour of this somewhat unfamiliar property.

Fig. 5 shows the change in geopotential height as a function of refractivity. From refractivity level 100 10^{-6} (i.e. in the lower stratosphere and above), the changes in geopotential height increase strongly with altitude (decreasing refractivity), and the seasonal variations are small.

The local behaviour of the annual means of refractivity at the geopotential heights 5, 15 and 20 km are shown in Figure 7 for the last 10 years of the climate simulation minus the the first 10 years. The

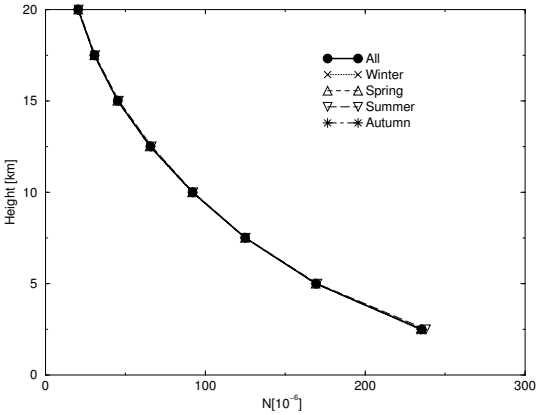

a. Global mean refractivity.

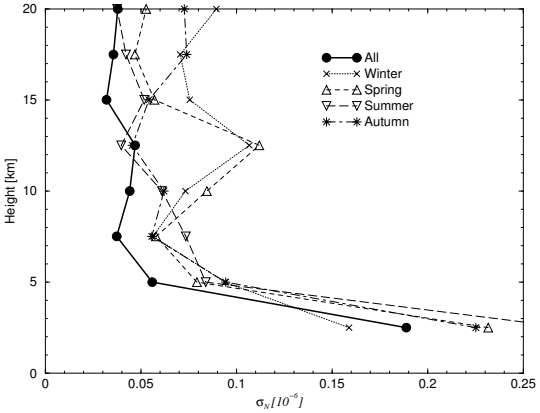

b. Inter-annual variation.

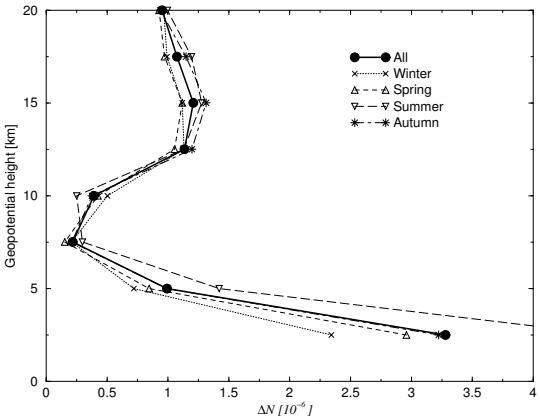

c. Climate evolution.

Figure 4. Variation of global mean refractivity of geopotential height surfaces

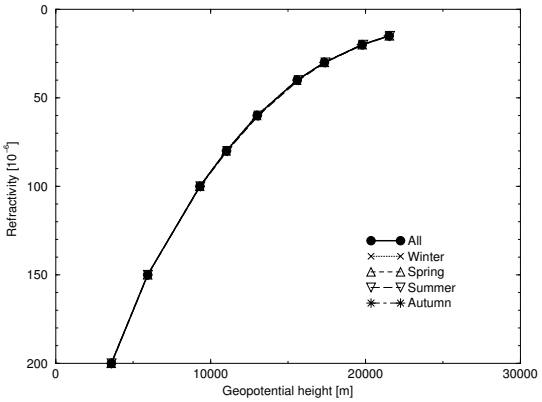

a. Global mean.

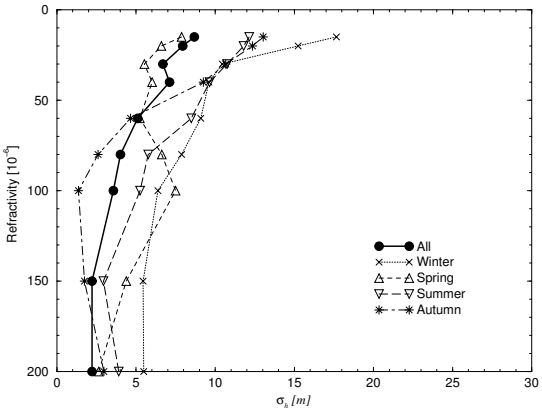

b. Inter-annual variation.

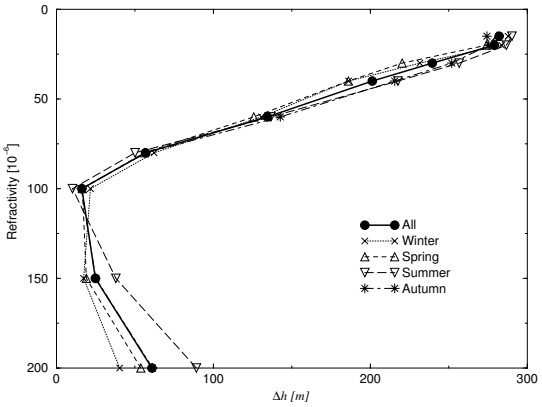

c. Climate evolution.

Figure 5. Variation of global mean geopotential height of refractivity surfaces

corresponding interannual variations are shown in Fig. 6. (When intercomparing the maps notice that the scales vary from plot to plot.)

At 20 km (Fig.7-a) changes are systematically positive and largest in the tropics. In the lower stratosphere (15 km, Fig.7-b) the changes in refractivity are again systematically positive, but now largest in the subtropics. As the height increases, the inter-annual variation (Fig. 6-a and -b) decreases systematically, both in absolute terms, but also, and more importantly, relative to the expected signal due to climate change.

Table I shows the values and variations of the global means of ZTD, ZWD, and IWV. There is a significant change in ZTD, nearly entirely due to a change in the wet component, ZWD. This is reflected in a corresponding change in IWV, which is, however, not directly measurable by means of GNSS observations. The regional changes and inter-annual variation of ZTD are shown in Fig. 8.

Table I. Behaviour of global means of ZTD, ZWD, and IWV

	Current	Future	Evolution	Inter-annual var.	Unit
ZTD	2.324	2.358	0.034	0.0011	m
ZWD	0.123	0.157	0.034	0.0010	m
ZHD	2.202	2.201	-0.0009	0.0005	m
IWV	19.71	25.47	5.76	0.17	mm

4. Discussion

In the study by Yuan et al. (1993) climate simulation data covering a summer and a winter month with and without a doubling of the CO_2 content were used to access the expected evolution of various GNSS measures due to climate change. For refractivity as function of height and ZTD it is possible to compare the expected changes with those of the present study. Qualitatively there is a fine agreement. Quantitatively the agreement is better than what could be expected, given the differences in climate models, amount of data, and periods of the year covered. It therefore appears that these GNSS measures are rather robust against the details of climate models, which is of great importance if they shall be useful in climate monitoring.

In the troposphere, there is a distinct climate change signal in refractivity, which crucially depends on humidity. This can be seen by

comparing Fig. 8-b (which is almost exclusively showing changes in humidity, as can be seen from Table I) and Fig. 7-c. Therefore a regional analysis is necessary to obtain a good sensitivity. Above the tropopause, the changes in refractivity vary less spatially, (Fig. 7-a and -b) and the global mean is a suitable approximation. In other words, a relatively small number of observations at these notoriously data-sparse levels will be sufficient for climate monitoring purposes. By comparing with Fig. 2, it appears that the changes in global mean refractivity are as significant relative to the annual variations as are changes in temperature.

Increases in temperature and humidity both expand a given layer (Eq. 3), and since the effect upon geopotential height is integral, geopotential height of isobaric surfaces just below the tropopause would be a suitable candidate to monitor climate change. Unfortunately, the existing records are pretty short and not very precise. GNSS RO observations can be used to derive this quantity, but, as demonstrated above and further discussed below, this may be neither necessary nor optimal.

Judging from Fig. 4-b and 4-c, the changes of geopotential height of constant refractivity surfaces due to global warming are expected to be as large and as significant in the middle and upper troposphere as the changes of geopotential height of isobaric levels, Fig. 3-a and 3-b. In the stratosphere the figures indicate that they are are even larger.

We here give an argument why refractivity versus height is a more sensitive measure in the stratosphere than is pressure versus height. From the analysis of the climate simulation it is known that the altitude of all pressure levels is increased, even in the stratosphere (Fig. 3-b). Specific humidity is decreasing with height; above a certain level, somewhere in the lower stratosphere, the effect of humidity upon refractivity and height becomes negligible. From Fig. 2-b one sees that above the tropopause the temperature decreases with height and the decrease in increasing upward. From Eq. 4 one sees that at constant pressure and negligible humidity this leads to an increase in refractivity. Therefore, to stay at an iso refractivity rather than isobaric surface one has to move even further up, resulting in an even larger height increment.

Thus, both from our analysis of the climate model data and from our theoretical argument we find that in the stratosphere the height of refractivity surfaces will be a more sensitive measure of global warming than the height of isobaric surfaces. Further down, near the tropopause, where humidity cannot be neglected, the measures will be equally sensitive, whereas in the lower troposphere the global mean height of iso refractivity surfaces is not well suited as a climate measure.

While the processing of GNSS RO observations into refractivity-height profiles does not rely on detailed information about the at-

mosphere it does involve an assumption about the atmosphere being spherically symmetric locally (in terms of the refractivity field in the section passed by the radio-waves), when the processing is done as presented here. As the Abel transformation is started from above, the assumption regards the local atmosphere from the altitude one is considering and up – not the atmosphere below. In reality the approximation does not hold entirely, but the deviations are not expected to be significant in the mid and in particular the high atmosphere. In the lower troposphere the existence of frontal zones and more local inhomogeneities in the water vapour distribution makes use of GNSS RO observations less straight forward, though work is under way to tackle such problems. It is therefore especially in the stratosphere and upper troposphere that direct use of the type of refractivity-height GNSS RO product discussed here can be expected to be useful.

Obviously it takes some analyses of climate models to couple changes in an unfamiliar measure like refractivity versus height to what is named "global warming". Is it best to process the GNSS RO data further into pressures and temperatures and analyse directly for global warming or to monitor refractivity and interpret the results via climate models?

This is a fundamental question when using atmospheric data in connection with atmospheric models, in particular when assimilating observations into numerical weather prediction (NWP) models. One has to balance several aspects: 1) Preprocessing involves assumptions and/or extra data, which may degrade the quality and independence of the observations. If the assumptions and/or data can be deduced from information which is in the model they are meant for and are less precise, it is clear that preprocessing should be avoided. 2) It may be impossible, however, to determine the model expectations for a given type of observation in its raw form from the model data. MSU radiances for models which do not go high enough is an example. Or it may be just unpractical, e.g. due to cpu-time reasons. GNSS RO bending angles is an example. This calls for preprocessing, even though theoretically it should be avoided. The general finding in NWP data assimilation is that one should preprocess as little as practically possible. In other words: In general one should convert from model space to observation space when comparing.

From table I it is tempting to conclude that use of global averages of ZTD are well suited for climate monitoring. However, contrary to the situations with occultation data obtained from LEO satellites, the ground based GNSS ZTD data will not have a homogenous global coverage. Like traditional synop data they are/will come mostly from more developed countries. Judging from Fig 8 there is a good sensitivity

at mid latitudes though, making it relevant to use ZTD data from, e.g., Europe and North America for climate monitoring. Further such data will provide an important means for validating and improving climate models, in particular high resolution regional climate models. Obviously proper handling of humidity is important in such models, but due to lack of data is has so far been difficult to access their skill regarding the treatment of water vapour.

5. Conclusion

We have analysed the changes of the GNSS RO measure refractivity versus height in response to "climate change". This was done using data from a recent "state of the art" simulation based on a fully coupled atmosphere ocean general circulation model. The evolution of the concentrations of greenhouse gases, CFCs and sulphur emissions follows the SRES scenario A2. The simulation covers 110 years, whereof the first 10 have been used to represent current climate and the last 10 future climate.

We have found that refractivity does change as a function of climate, and that the magnitude of change makes the use of refractivity as a function of height highly useful for monitoring climate change.

In the stratosphere the height of iso-refractivity surfaces increases systematically in response to global warming. The inter-annual variability is relatively low at these levels. In the upper part of the model atmosphere, where humidity is negligible, our analysis indicates that refractivity is even better suited than pressure as a reference surface for height. A theoretical argument in support of that is given in the discussion. This makes the use of height versus refractivity very promising in the stratosphere. Further adding to this is the fact that in the upper atmosphere the spatial variations are smaller than in the low atmosphere. Thus, besides the sensitivity being larger, fewer observations are needed to determine from observations a mean global (or regional) value with a given precision.

In the mid and low troposphere we find large, mainly latitude-dependent, variations in the change of refractivity. These variations include even the change of the sign. Monitoring climate change using refractivity as function of height in the troposphere therefore requires the use of regional averages or maps rather than global averages. Further studies are necessary in order to find the optimal way of making such local averages and comparing to output from climate simulations.

GNSS RO observations can be processed into profiles of pressure, temperature and humidity. But this requires additional assumptions,

wherefore it appears more robust to use the data more directly in the form of refractivity versus height when monitoring climate be means of GNSS RO data. This in-dependency of the refractivity-height GNSS RO product will enable control of the outcome of climate monitoring campaigns based on other data.

GNSS RO data are further well suited for assimilation into NWP models, where they can be expected to alleviate some current calibration problems with satellite observations. In the future, GNSS RO observations will therefore likely become available for climate monitoring also in a more indirect form: via inclusion in the observations used in re-analysis projects.

Using the same climate model data, it is furthermore found that also data from ground-based GNSS receivers are well suited for climate research.

Acknowledgements

We wish to thank Eigil Kaas, DMI, for important comments to the work, and Leif Laursen, DMI, for comments to the manuscript. This work was started as part of the ACE Scientific Support Study funded by ESA, ESTEC Contract No 14809/00/NL/MM, for which H.V. is thankful.

References

Bevis, M., T. A. Herring, R. A. Anthes, C. Rocken, and R. H. Ware: 1994, 'GPS Meteorology: Mapping Zenith Wet Delays onto Precipitable Water'. *Jour. Appl. Met.* **33**, 379.

Healy, S. B. and J. R. Eyre: 2000, 'Retrieving temperature, water vapour and surface pressure information from refractive-index profiles derived by radio occultation: A simulation study'. *Q. J. R. Meteorol. Soc.* **126**, 1661.

Kuo, Y. H.: 2000, 'Assimilation of GPS Radio Occultation Data for Numerical Weather Prediction'. *TAO* **11**, 157.

Leroy, S. S.: 1997, 'Measurements of geopotential height by GPS radio occultation.'. *Journal of Geophysical Research* **102**(D6), 6971.

Meincke, M. D.: 1999, 'Inversion Methods for Atmospheric Profiling with GPS Occultations'. Scientific report 99-11, Danish Meteorological Institute. (Ph.D. thesis).

Nakicenovic, N., O. Davidson, G. Davis, A. Grübler, T. Kram, E. L. L. Rovere, B. Metz, T. Morita, W. Pepper, H. Pitcher, A. Sankonski, P. Shukla, R. Swart, R. Watson, and Z. Dadi: 2000, 'Emission scenarios. Summary for policymakers. A special report of IPCC working group III'. ISBN 92-9169-113-5.

Oberhuber, J. M.: 1993, 'Simulation of the Atlantic circulation with a coupled sea ice-mixed layer isopycnal general circulation model. Part I: Model description'. *J. Phys. Oceanogr.* **22**, 808.

Roeckner, E., K. Arpe, L. Bengtsson, M. Christoph, M. Claussen, L. Dümenil, M. Esch, M. Giorgetta, U. Schlese, and U. Schulzweida: 1996, 'The atmosphere general circulation model ECHAM-4: Model description and simulation of present-day climate'. Technical report, Max Planck Institut für Meteorologie. Report 218.

Santer, B. D., K. E. Taylor, T. M. L. Wigley, T. C. Johns, P. D. Jones, D. J. Karoly, J. F. B. Mitchell, A. H. Oort, J. E. Penner, V. Ramaswamy, M. D. Schwarzkopf, R. J. Stouffer, and S. F. B. Tett: 1996, 'A search for human influences on the thermal structure of the atmosphere'. *Nature* **382**, 39–46.

Stendel, M., T. Schmith, E. Roeckner, and U. Cubasch: 2000, 'The Climate of the 21'st century: Transient simulations with a coupled atmosphere-ocean general circulation model'. Technical report, Danish Climate Centre, Danish Meteorological Institute. Report 00-6.

Tett, S. F. B., J. F. B. Mitchell, D. E. Parker, and M. R. Allen: 1996, 'Human influence on the atmospheric vertical temperature structure: detection and observations'. *Science* **274**, 1170–1173.

Vedel, H.: 2000, 'Conversion of WGS84 geometric heights to NWP model HIRLAM geopotential Heights'. DMI scientific rapport 00-04, Danish Meteorological Institute.

Yuan, L. L., R. A. Anthes, R. H. Ware, C. Rocken, W. D. Bonner, M. G. Bevis, and S. Bursinger: 1993, 'Sensing Climate Change Using the Global Positoining System'. *J.G.R.* **98**(D8), 14925–14937.

Zou, X., B. Wang, H. Liu, R. A. Anthes, T. Matsumura, and Y.-J. Zhu: 2000, 'Use of GPS/MET refraction angles in three-dimensional variational analysis'. *Q. J. R. Meteorol. Soc.*

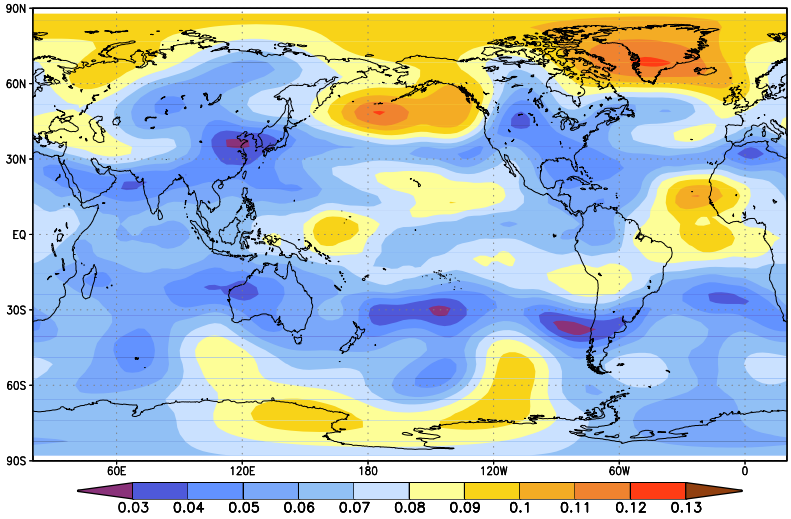

a. 20 km.

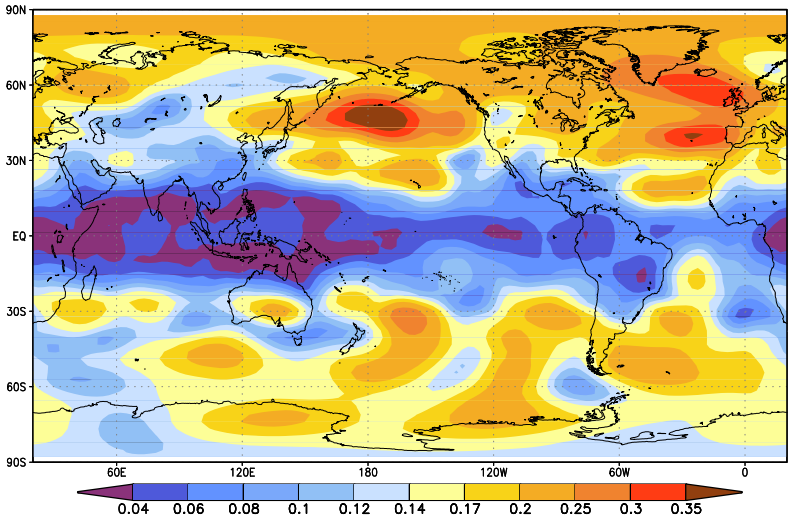

b. 15 km.

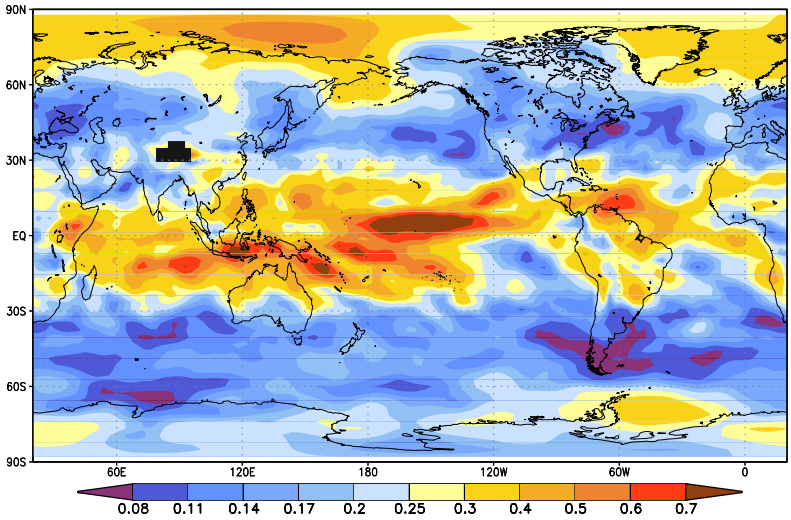

c. 5 km.

Figure 6. Interannual variation of refractivity at different geopotential heights.

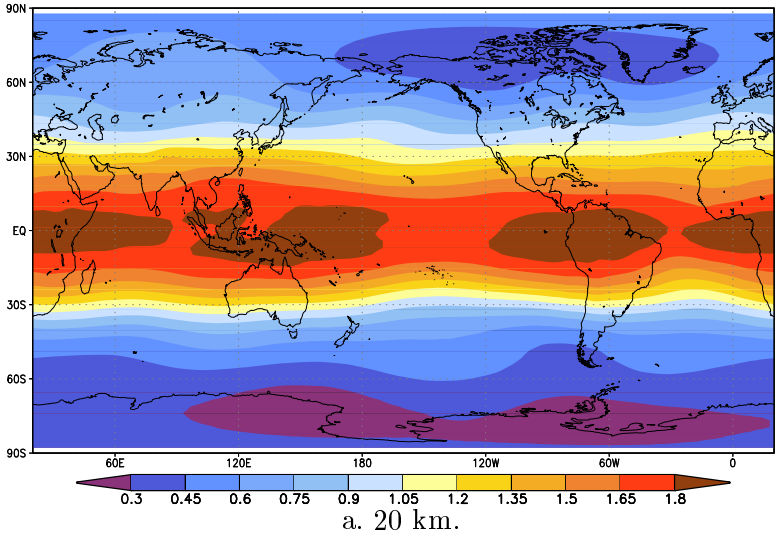

a. 20 km.

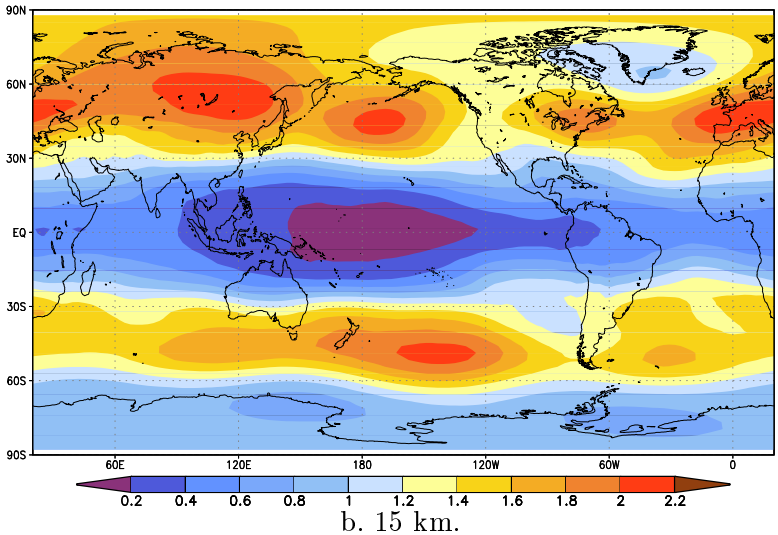

b. 15 km.

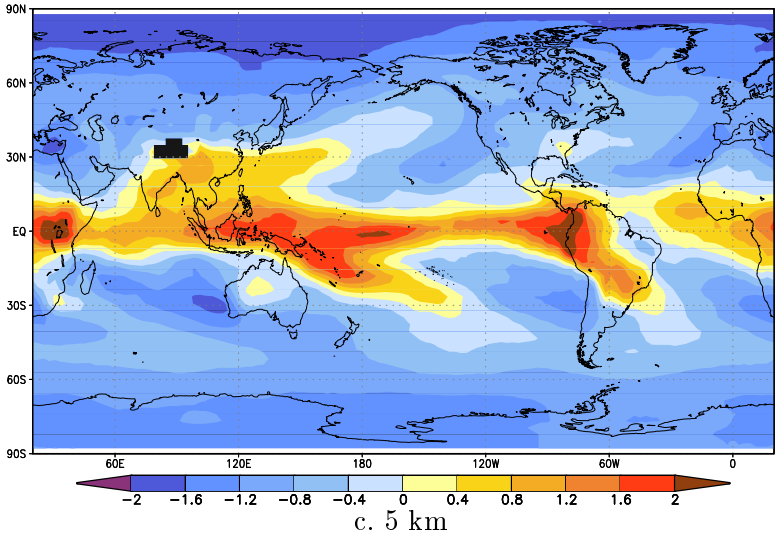

c. 5 km

Figure 7. Climate induced variation of refractivity at different geopotential heights.

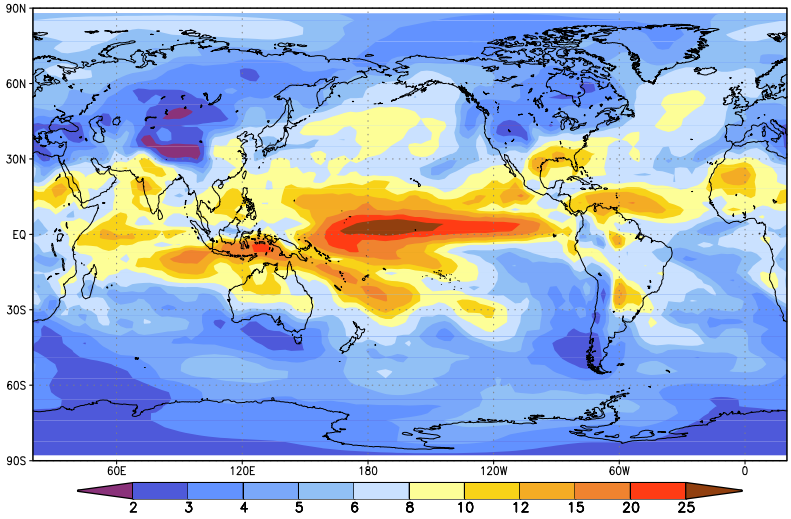

a. ZTD inter-annual variations [mm]

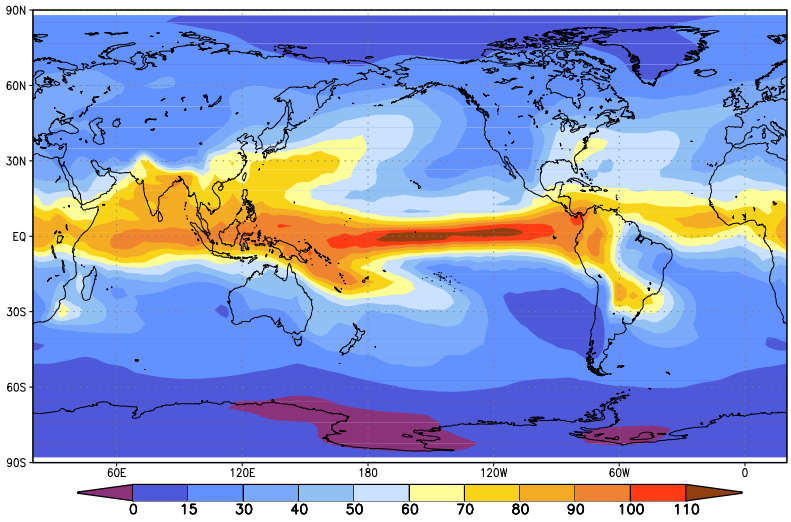

b. ZTD evolution [mm]

Figure 8. Climate induced variation of ZTD